J. Fluid Mech. (1982), *vol.* 118, *pp.* 59–77
Printed in Great Britain

An experimental study of the wall-pressure field associated with a turbulent spot in a laminar boundary layer

By T. S. MAUTNER†
Naval Ocean Systems Center, San Diego, California 92152, U.S.A.

AND C. W. VAN ATTA†
Scripps Institution of Oceanography, University of California, San Diego, La Jolla, California 92093, U.S.A.

(Received 5 January 1981 and in revised form 18 August 1981)

Wall-pressure fluctuations were measured in the plane of symmetry and five off-axis positions in artificially generated turbulent spots in a laminar boundary layer. Ensemble averages of the wall-pressure signatures show that the spot's pressure signature is characterized by two positive-pressure peaks and a central negative-pressure region along the centre line which evolves into one negative- and one positive-pressure perturbation in the wing-tip region. In similarity co-ordinates, based on pressure-signature characteristics, the spatial growth of the pressure signature shows a small Reynolds-number dependence. Contours of the ensemble-averaged wall pressure measured relative to the laminar value show that a turbulent spot produces a leading-edge pressure excess followed by a pressure-defect region having its maximum values at the spot wing tips. The trailing edge of the pressure disturbance was found to consist of a spanwise region of pressure excess, also having its maximum value at the wing tips.

1. Introduction

The recent measurements by Cantwell, Coles & Dimotakis (1978) and Savas (1979) of the structure of turbulent spots in a flat-plate laminar boundary layer resulted in two representations of the turbulent spot wall-pressure field. Cantwell *et al.* inferred the centre-line spot pressure signature by using the conical property of the spot's velocity field, the non-steady Bernoulli equation, and the measured free-stream velocity perturbation ($x = 89$ and 119 cm, $U_\infty = 0{\cdot}59$ m/s, $R_{ex} \simeq 5{\cdot}8 \times 10^5$ and $7{\cdot}8 \times 10^5$, water). Savas measured the wall pressure at one streamwise location and velocity in the plane of symmetry of the spot ($x = 84{\cdot}6$ cm, $U_\infty = 10$ m/s, $R_{ex} \simeq 5{\cdot}5 \times 10^5$, air). The wall-pressure signature of Savas is characterized by a positive-pressure peak ($C_p \simeq 0{\cdot}005$) at the spot's leading edge, a central negative peak ($C_p \simeq -0{\cdot}01$) and a final positive peak ($C_p \simeq 0{\cdot}18$) occurring just prior to the spot's trailing edge. In contrast, the wall-pressure disturbance inferred by Cantwell *et al.* is initially negative, reaching a minimum ($C_p \simeq -0{\cdot}0035$) at the leading edge. The pressure then increases, reaching a maximum positive value ($C_p \simeq 0{\cdot}005$) at the trailing edge. The differences

† Also at Department of Applied Mechanics and Engineering Sciences, University of California, San Diego.

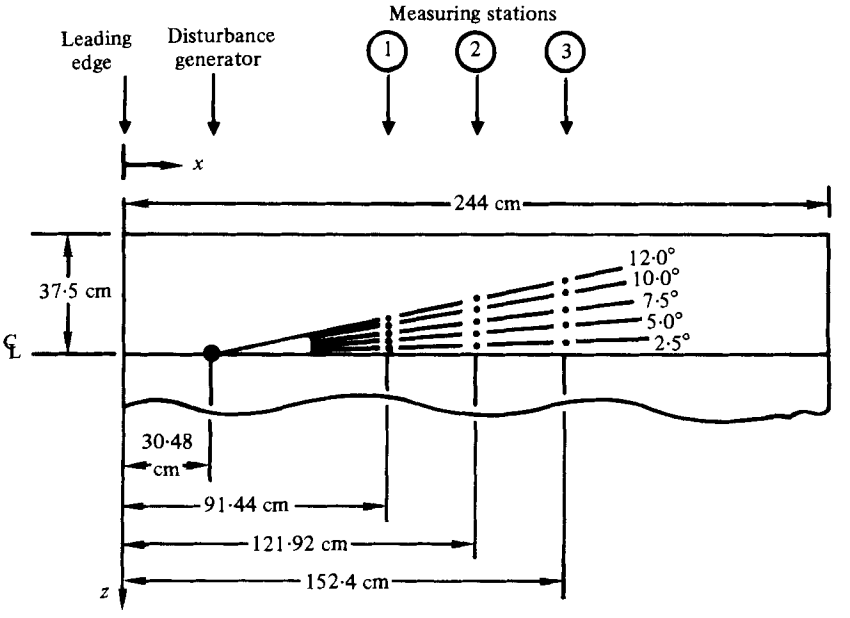

FIGURE 1. Plan view of the flat-plate model showing co-ordinate system, dimensions and measuring stations.

between the two signals indicate the need for comprehensive measurements to define more completely the spatial distribution of the spot's wall-pressure field.

The pressure measurements made thus far have not established the variation of the wall-pressure field within the spot as a function of streamwise and spanwise position and free-stream velocity. It is not known if the wall-pressure signature of the spot has a universal structure, if it exhibits similarity or if it correlates in a one-to-one correspondence with the spot's velocity signature as reported by Wygnanski, Sokolov & Friedman (1976), Cantwell *et al.* (1978) and others.

Experiments conducted by DeMetz & Casarella (1973), Huang & Hannan (1975) and Gedney (1979) have established certain statistical properties, in terms of intermittency, of the wall-pressure fluctuations during natural transition. It is not possible to infer individual spot wall-pressure characteristics from these measurements since the turbulent spots were occurring randomly and the measurements were made at uncontrollable locations within the spots.

The purpose of this paper is to report experimental data on the wall-pressure field $P(x, z, t)$ associated with artificially generated turbulent spots in a flat-plate laminar boundary layer. The large-scale structure and predominant characteristics of the wall-pressure signatures are determined from ensemble-averaged wall-pressure distributions at six transverse locations for each of the three streamwise positions and two free-stream velocities. The ensemble-averaged pressure signals are transformed into similarity coordinates for comparison with the results of Cantwell *et al.* and Savas, and an attempt is made to qualitatively identify the relationship between the spot's velocity and wall-pressure fields.

2. Experimental apparatus and conditions

The measurements were made in the low-speed, low-turbulence, closed-circuit wind tunnel in the Department of Applied Mechanics and Engineering Sciences at the University of California at San Diego. The test section was 76 cm × 76 cm × 10 m, and the flat-plate model was mounted on jacks in a nearly horizontal position (angle of attack $\simeq -0{\cdot}34°$) at the height of approximately 24 cm above the tunnel floor, with the leading edge located at the entrance of the test section. The longitudinal-turbulence level U'/U_∞ in the test section is less than 0·05 % at 10 m/s.

The test plate and its leading edge were constructed separately from type 300 aluminium tool and jig plate. The leading-edge section had an overall steamwise length of 10 cm and was machined to include a wedge angle of 9·0° extending 7·6 cm downstream and joining smoothly the constant-thickness section. The flat plate is 1·27 cm thick and 75 cm wide with an overall length of 2·44 m. After mounting the leading edge, all joints were filled and the plate was polished to a mirror-like finish.

The velocity and pressure measurements were made at three stations located at $x = 91{\cdot}4$, 121·9 and 152·4 cm from the leading edge at free-stream velocities $U_\infty = 7{\cdot}8$ and 10·1 m/s. At each station, a centre-line ($z = 0$) and five off-axis measurements were made along rays originating at the turbulent-spot generator as shown in figure 1. Since the lateral growth of the spot in x is linear, starting approximately at the disturbance generator, measurements along each ray at its respective angle θ provides data at the same relative spanwise location within the spot at each x-location.

The turbulent-spot generator consisted of a 5 cm diameter audio speaker located at $x = 30{\cdot}5$ cm downstream of the leading edge. The speaker was mounted on the bottom of the plate and, when driven by a square-wave pulse having an amplitude of 10 V and duration of 100 μs, pushed a jet of air through a 0·32 cm diameter hole in the plate. A turbulent spot was generated every 1·5 s.

The free-stream velocity was monitored with a Pitot static tube connected to an MKS Baratron pressure transducer. The instantaneous longitudinal velocity was measured using a TSI 1040 constant-temperature anemometer and a TSI 1210 hot wire. The hot-wire probe was attached to an airfoil-shaped strut which was connected to a traversing mechanism through sealed slots in the wind tunnel wall. The vertical (y) location of the probe was determined using a telescope cathetometer. The hot wire was calibrated in the free stream at each measurement location before and after each run. The laminar mean-velocity profiles were measured at the three x-stations for $U_\infty = 7{\cdot}8$ and 10·1 m/s and are compared to the theoretical Blasius profile in figure 2. In addition to the turbulent-spot velocity field along the centre line, velocity measurements were made at several off-axis stations on both sides of the plate to verify symmetry of the flow with and without turbulent spots.

The pressure distribution along the plate was adjusted to positioning a 30·5 cm long airfoil-shaped trailing edge flap at 12° above the horizontal. The upward flap deflection produces a slight overpressure on the working surface, and the gap between the plate edge and the tunnel wall allows a small flow of air through the gap. This configuration would eliminate, or at least suppress, transverse contamination from the leading edge. No transverse contamination was observed in the velocity or pressure measurements. Static-pressure measurements were made at both the streamwise and spanwise measurement locations using pressure taps along the plate's surface. The pressure was

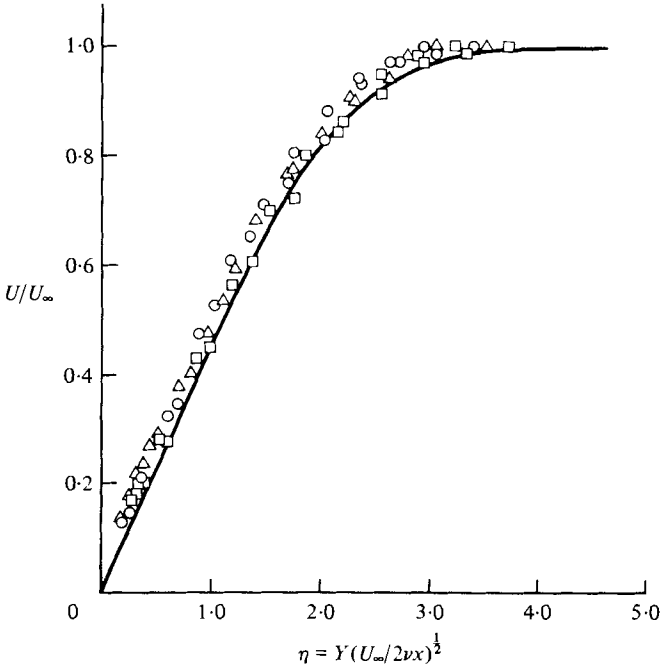

FIGURE 2. Measured laminar velocity profiles for U_∞ = 7·8 and 10·1 m/s. □, x = 91·4 cm; ○, 121·9 cm; △, 152·4 cm; ——, theoretical Blasius profile.

nearly uniform over the measuring region and with maximum pressure gradient of $\Delta C_p/\Delta x = 4 \times 10^{-4}\,\mathrm{cm}^{-1}$ for U_∞ = 7·8 m/s and $\Delta C_p/\Delta x = 1 \times 10^{-4}\,\mathrm{cm}^{-1}$ for U_∞ = 10·1 m/s, where $C_p = 2(P - P_\infty)/\rho U_\infty^2$.

The wall-pressure fluctuations were measured using a B & K Model 4138 0·32 cm diameter condenser microphone whose sensing area was reduced by using a 0·8 mm diameter pinhole in the plate's surface which led to a 0·8 mm thick, 0·32 cm diameter cavity above the microphone diaphragm. The microphone was connected to a B & K 2619 preamplifier and was driven by a B & K 2609 measuring amplifier. The pressure sensitivity at 1000 Hz was determined using a B & K Model 4230 pistonphone, which produced an effective free-field sound level of 94 dB. The microphone was calibrated at each measuring location and had a nominal sensitivity of $-62{\cdot}5 \pm 1$ dB re 1 V/Pa. Spectral analysis of the microphone signals showed that there were no resonant frequencies present in the range of experimental conditions.

3. Data reduction

The experimental data was recorded on a Sangamo Sabre III, 14 channel FM analog tape recorder. The hot-wire voltages were recorded after being passed through a buck-and-gain amplifier and the microphone signals were recorded directly from the measuring amplifier. The square-wave trigger signal for the spot generator was also recorded and used to trigger and synchronize the digitizing operation. The analog signals were played back at the recording speed of 76·2 cm/s and digitized using a 12 bit plus-sign A/D converter at a sampling rate of 7500 Hz.

Each velocity and pressure realization was represented by 2048 digital samples

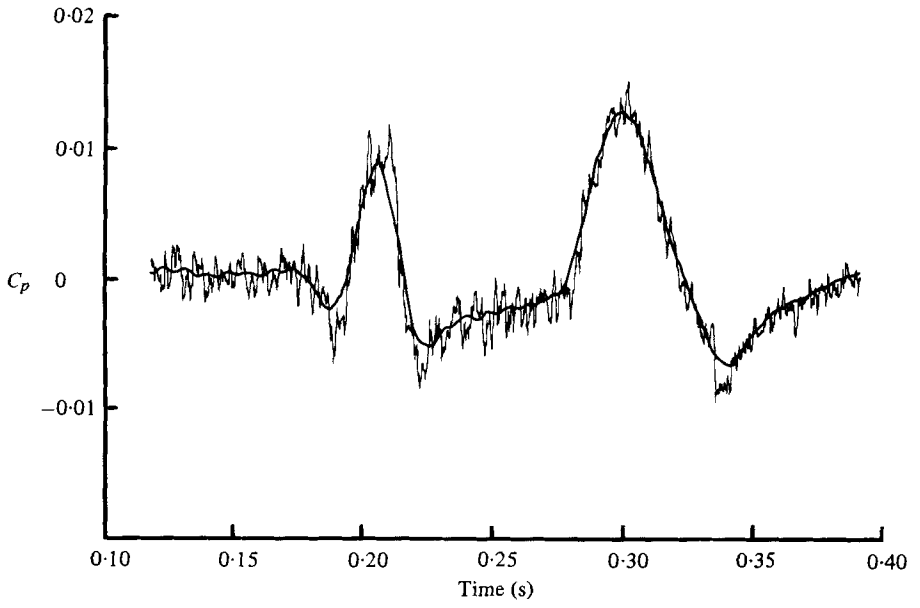

FIGURE 3. Comparison of a typical filtered and unfiltered ensemble-averaged pressure signal. $x = 152{\cdot}4$ cm, $z = 0$, $U_\infty = 10{\cdot}1$ m/s.

taken after a fixed time delay following each trigger pulse. Then the ensemble mean velocity U and wall-pressure-coefficient C_p signatures were formed by averaging over 100 spots for the velocity and 500 spots for the pressure. For the pressure record from each spot C_{pi}, the fluctuation about the ensemble mean C_p is defined as $C_{pi}-C_p$, and has an ensemble-mean value of zero. The r.m.s. ensemble-averaged value C'_p of this fluctuation was calculated from each sampling time t. This furnished a measure of the variation over different spots used in the ensemble average and may be interpreted as a turbulent intensity relative to the ensemble mean. The ensemble-mean pressure signals were digitally filtered using a low-pass smoothing filter set at 240 Hz. A comparison of a typical filtered and unfiltered ensemble-mean wall-pressure signal is shown in figure 3.

4. Results and discussion

The ensemble-mean pressure signatures observed at the three measuring stations $x = 91{\cdot}4$, $121{\cdot}9$ and $152{\cdot}4$ cm are plotted, in figures 4 and 5, in terms of C_p as a function of time for six spanwise locations z/b and free-stream velocities $U_\infty = 7{\cdot}8$ and $10{\cdot}1$ m/s, where $z/b = \tan\theta/\tan 10°$. Relative to ambient, the wall pressure along the spot's centre line is characterized by a small pressure decrease followed by a sharp pressure rise, a central negative-pressure region, a second positive-pressure peak and relaxation back to the laminar value. As the spot is convected downstream, the central negative-pressure region increases in length, while the magnitude decreases and becomes nearly constant at $x = 152{\cdot}4$ cm. This indicates that the pressure defect in the centre region of the spot is following the general shape of the velocity excess near the wall (see figure 11 of Cantwell *et al.* 1978).

For increasing values of z/b, the magnitude of both the initial negative pressure

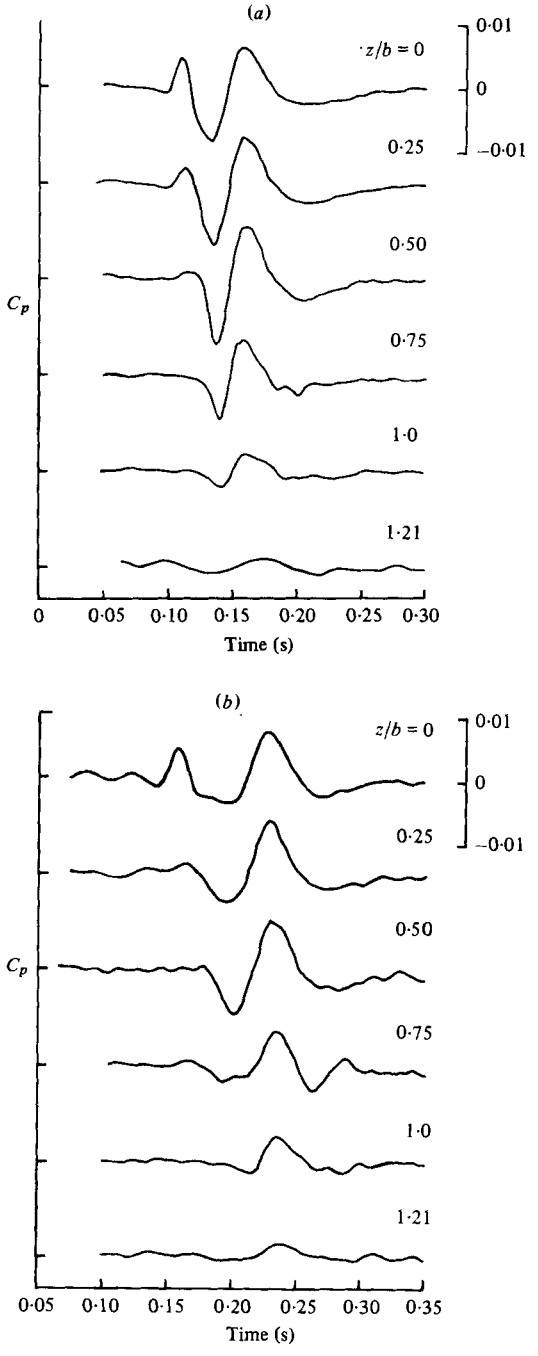

FIGURE 4 (*a*, *b*). For caption see opposite page.

and the first positive wall-pressure perturbations are reduced, and the wing-tip region of the spot's pressure signature becomes characterized by one negative and one positive pressure perturbation. The centre-line negative-pressure region which had been elongated and flattened with increasing x, now, for increasing z/b, shortens and becomes increasingly negative, reaching a maximum at $z/b = 0{\cdot}50$–$0{\cdot}75$. The second

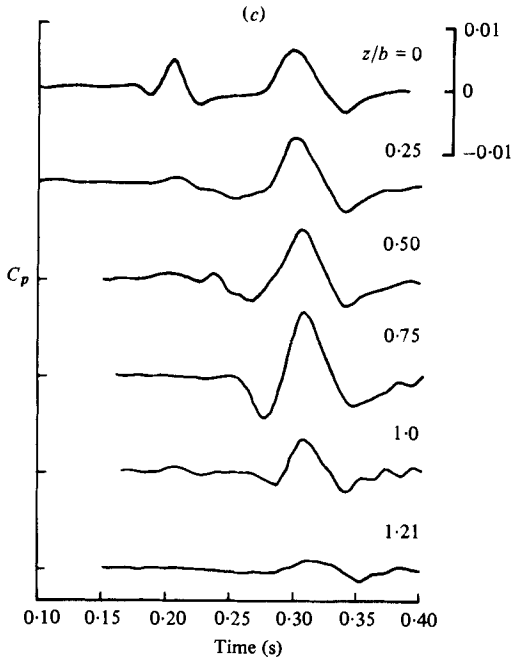

FIGURE 4. Ensemble-mean C_p as a function of time for various z/b at $U_\infty = 7{\cdot}8$ m/s. (*a*) $x = 91{\cdot}4$ cm; (*b*) 121·9 cm; (*c*) 152·4 cm.

positive-pressure peak remains coherent across the spot and also has a maximum in the region of $z/b = 0{\cdot}50$–$0{\cdot}75$. The reduction in magnitude and final disappearance of the first negative and positive pressure perturbations, with increasing z/b, produces a swept-back shape in the spot's pressure-field leading edge, while the coherent second positive peak produces a nearly constant value of x versus z for the location of the trailing edge. The resulting planform shape of the spot's pressure field is similar to that obtained from the velocity measurements of Wygnanski *et al.* (1976), who reported that the spot's velocity disturbance in the plan view has a triangular shape with a blunt trailing edge near the wall. The spanwise growth of the spot's velocity disturbance has been reported by Wygnanski *et al.* and by Schubauer & Klebanoff (1956) to be 10°, and the current velocity measurements indicate a maximum spanwise growth of approximately 10° as measured by the intermittent passage of the velocity disturbance in the spot's wing-tip region. The ensemble wall-pressure signal at $z/b = 1{\cdot}21$ ($\theta = 12°$) indicates that the wall-pressure signature has a spanwise growth more nearly equal to 12°, so that the velocity perturbations, spreading with an angle of approximately 10°, induce a pressure-disturbance field outside and ahead of the velocity-disturbance spanwise interface.

To test the space–time similarity of the spot's wall-pressure signature, the time co-ordinate of the ensemble-mean C_p data was transformed using the similarity co-ordinate ξ introduced by Cantwell *et al.* (1978), where $\xi = (x-x_0)/U_\infty(t-t_0)$. The virtual origin (x_0, t_0) was determined by two methods. First, the graphical procedure of Cantwell *et al.* was used to determine the virtual origin (x_{0v}, t_{0v}) from the velocity measurements along $z = 0$, at the three x-locations, for $U_\infty = 10$ m/s. The insert in figure 6 illustrates the procedure used to identify characteristic points in each velocity

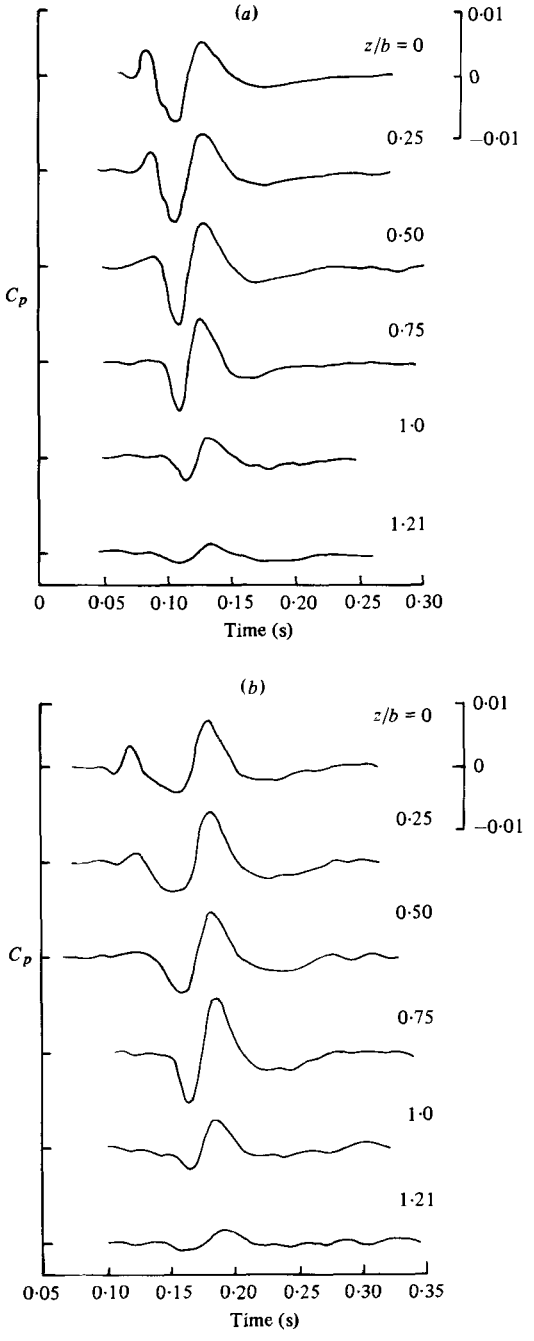

FIGURE 5 (*a*, *b*). For caption see opposite page.

signal, and the earliest arrival time of points A and B and the latest arrival time of points C and D are plotted in figure 6. Rays drawn through these points locate the velocity virtual origin at $x_{0v} = 0$ cm and $t_{0v} = -0{\cdot}035$ s and determine the celerity of leading and trailing edges to be $0{\cdot}87\ U_\infty$ and $0{\cdot}56\ U_\infty$ respectively.

A second graphical procedure was used to determine the virtual origin (x_{0p}, t_{0p}) of

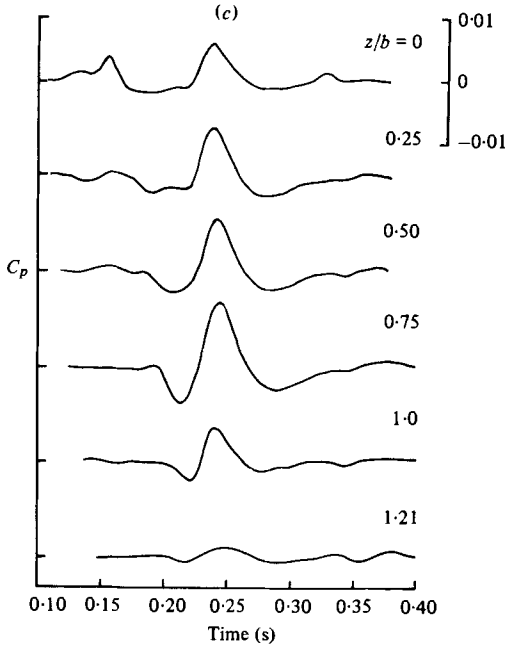

FIGURE 5. Ensemble-mean C_p as a function of time for various z/b at $U_\infty = 10{\cdot}1$ m/s. (*a*) $x = 91{\cdot}4$ cm; (*b*) 121·9 cm; (*c*) 152·4 cm.

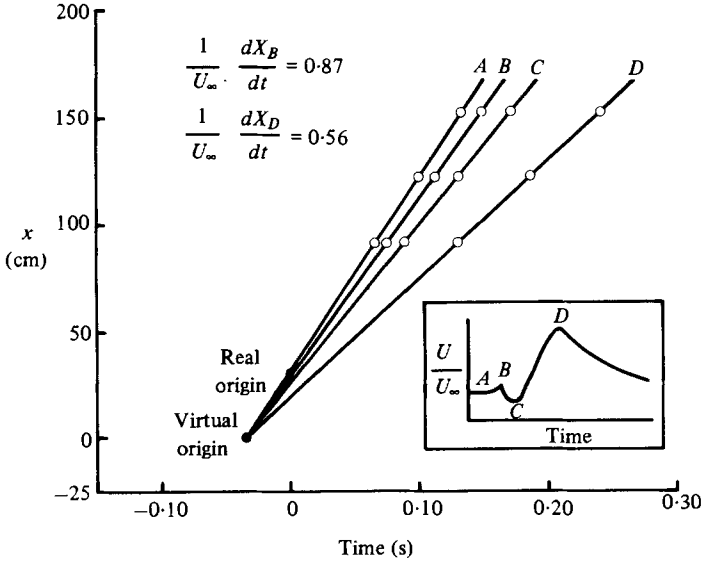

FIGURE 6. Determination of the velocity field's virtual origin and celerities for $U_\infty = 10$ m/s. Virtual origin is at $x_{0v} = 0$ cm, $t_{0v} = -0{\cdot}035$ s.

the wall-pressure field. The arrival times of the first and second positive peaks of the wall-pressure signals along $z = 0$ were measured at the three x-locations for both $U_\infty = 7{\cdot}8$ and $10{\cdot}1$ m/s. Rays drawn through these points locate the wall-pressure field virtual origin at $x_{0p} = 24$ cm and $t_{0p} = 0{\cdot}005$ s, as shown in figure 7. Rays drawn through the arrival times of the mid-points of the central negative-pressure peaks also

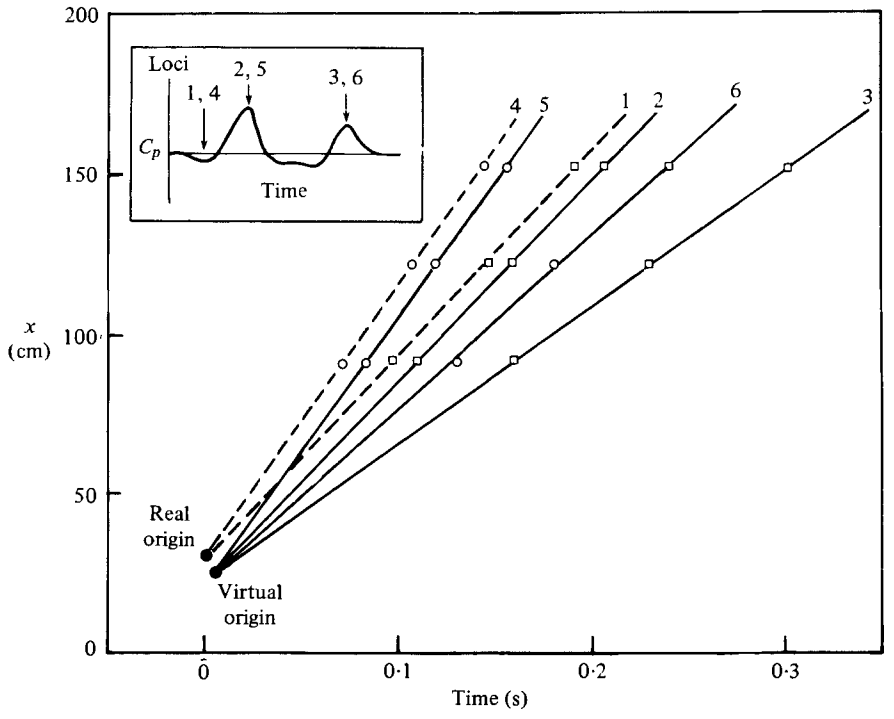

FIGURE 7. Determination of the wall-pressure virtual origin and celerities for U_∞ = 7·8 m/s (loci 1, 2, 3) and 10·1 m/s (loci 4, 5, 6). Virtual origin is at x_{0p} = 24 cm, t_{0p} = 0·005 s. Values of $U_\infty^{-1}\,dx/dt$ are as follows: locus (1), 0·83; (2), 0·81; (3), 0·55; (4), 0·85; (5), 0·84; (6), 0·54.

pass through the virtual origin (x_{0p}, t_{0p}). In figure 7, the rays numbered 1 and 4 represent the arrival times of the first pressure minimum points. The loci 1, 2, 4 and 5 are now associated with the leading edge of the spot's pressure-disturbance field and yield average celerities of $0{\cdot}82U_\infty$ and $0{\cdot}845U_\infty$ for U_∞ = 7·8 and 10·1 m/s respectively. Loci 3 and 6 are associated with the trailing-edge interface and produce celerities of $0{\cdot}55U_\infty$ and $0{\cdot}54U_\infty$ for U_∞ = 7·8 and 10·1 m/s.

The nearly equal celerity of loci 1 and 2 for U_∞ = 7·8 m/s and loci 4 and 5 for U_∞ = 10·1 m/s indicate that the leading-edge region of the pressure-disturbance field accompanies the arrival of both the velocity-disturbance leading-edge overhang (loci 1 and 4) and the velocity perturbation near the wall (loci 2 and 5). The equal celerity in the leading-edge region of the spot's pressure field is consistent with the results of Wygnanski *et al.* (1976) and Wygnanski (1980, private communication), who noted that the convection speed of the spot's velocity-disturbance leading edge is independent of the y-co-ordinate, but contradicts the notion of conical similarity of the wall-pressure field. For complete conical similarity, loci 1 and 4 would have to pass through the virtual origin (x_{0p}, t_{0p}).

Using each of the two virtual origins (x_{0v}, t_{0v}) and (x_{0p}, t_{0p}), the time co-ordinate of the ensemble-mean C_p signatures is transformed into the similarity variables ξ_v and ξ_p, where $\xi_v = (x-x_{0v})/U_\infty(t-t_{0v})$ and $\xi_p = (x-x_{0p})/U_\infty(t-t_{0p})$. The transformed pressure data along the centre line at the three measuring stations are shown in figures 8 and 9 for ξ_v and ξ_p respectively. An immediate consequence apparent in figure 8 is the failure of ξ_v to collapse the C_p signatures at the two free-stream velocities.

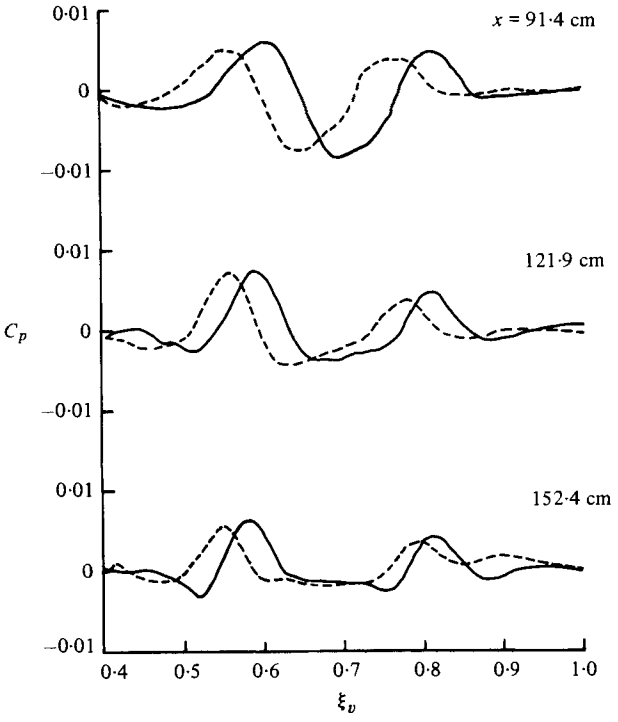

FIGURE 8. Ensemble-averaged mean C_p as a function of ξ_v along $z/b = 0$ using the virtual origin (x_{0v}, t_{0v}). ——, $U_\infty = 7{\cdot}8$ m/s; – – –, 10·1 m/s.

However, the C_p data do appreciably collapse toward each other when represented in terms of ξ_p. It should be noted that when the time co-ordinate of the wall-pressure signatures is transformed into either ξ_v or ξ_p, at a particular single value of the free-stream velocity, the C_p data exhibit an excellent degree of similarity, as indicated by the nearly constant location in ξ of the two positive-pressure peaks at the three x-locations. Although only the centre-line wall-pressure data has been presented in similarity co-ordinates, the above conclusions were also found to apply to the pressure signatures at the five off-centre-line spanwise locations.

If, in terms of ξ_p, one measures the spatial growth of the spot's wall-pressure field along the centre line by the separation of the two positive peaks, it is observed that the streamwise growth is greater at 10·1 m/s. As the differences in the turbulent spot's leading- and trailing-edge velocity-interface celerities produce streamwise spatial growth, the differences in the celerities at 7·8 and 10·1 m/s, obtained from figure 7, also demonstrate a larger spatial growth rate of the wall-pressure signature at 10·1 m/s. These results violate the premise of conical similarity and imply a Reynolds-number dependence in the characteristic features of the wall-pressure signature.

Figure 10 uses the similarity co-ordinate ξ to compare two representations of the turbulent spot's centre-line wall pressure. Cantwell *et al.* (1978) inferred the wall pressure from the conical property of the spot's velocity field, the non-steady Bernoulli equation and the measured free-stream velocity perturbation due to passage of the spot. The resulting signature predicts a central negative region and final positive peak that have comparable magnitude in C_p and location in ξ_p with the present measure-

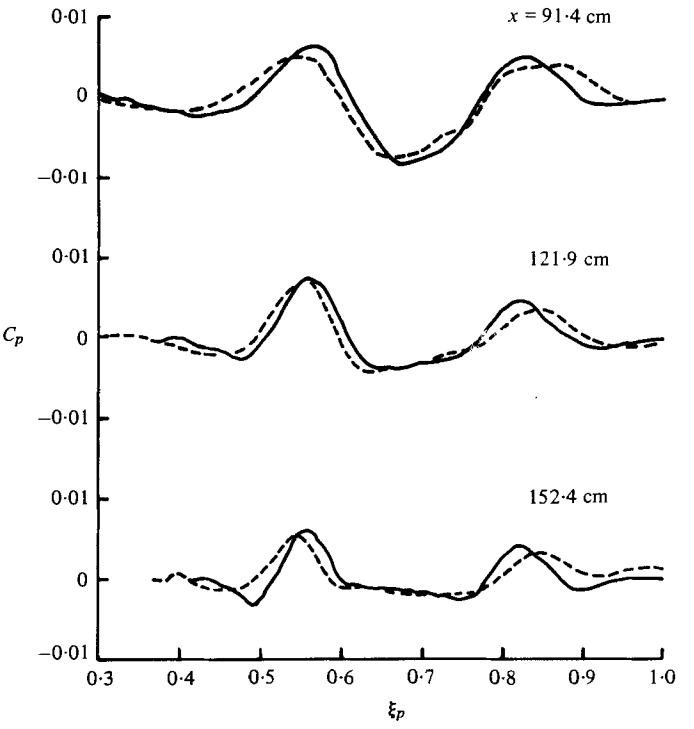

FIGURE 9. Ensemble-averaged mean C_p as a function of ξ_p along $z/b = 0$ using virtual origin (x_{0p}, t_{0p}). ——, $U_\infty = 7{\cdot}8$ m/s; – – –, 10·1 m/s.

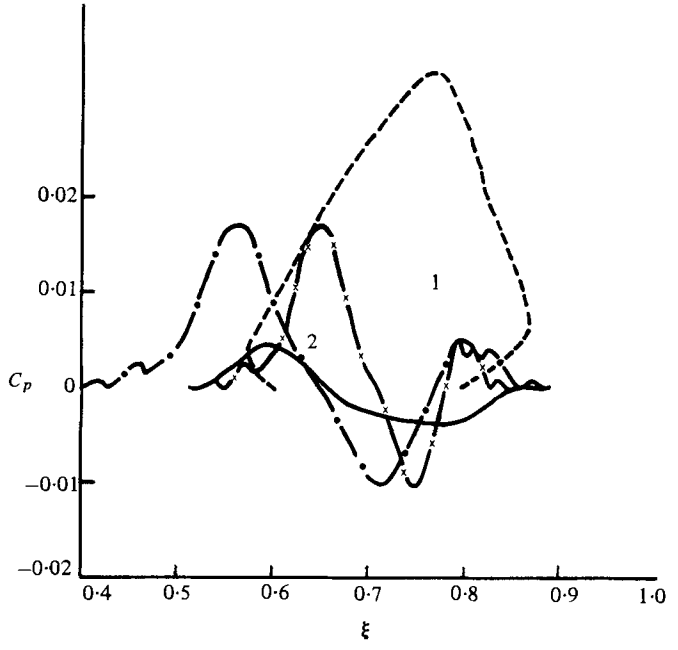

FIGURE 10. Comparison of the wall-pressure signature and spot outline of Cantwell *et al.* (1978) with the wall pressure measured by Savas (1979). ——, inferred wall pressure of Cantwell *et al.* ($U_\infty = 0{\cdot}59$ m/s, water); —×—, measured wall pressure of Savas ($U_\infty = 10$ m/s, $x = 84{\cdot}6$ cm, $x_0 = -30$ cm, $t_0 = -0{\cdot}063$ s, air); —●—, replot of Savas' data using $x_{0p} = 24$ cm, $t_{0p} = 0{\cdot}005$ s; points 1 and 2 are particle path accumulation points computed by Cantwell *et al.*

ments, but the method does not predict the first positive peak. One would conclude that accurate calculation of the wall-pressure field may require including the three-dimensionality of the associated velocity field.

The ensemble-mean C_p signature measured by Savas (1979) ($x = 84{\cdot}6$ cm, $U_\infty = 10$ m/s, $R_{ex} = 5{\cdot}5 \times 10^5$) was transformed into the ξ-co-ordinate using a virtual origin ($x_0 = -30$ cm, $t_0 = -0{\cdot}063$s) obtained from his velocity-field data. There is disagreement between the data of Savas and the signature inferred by Cantwell *et al.* Comparing the Savas data with the present measurement at $x = 91{\cdot}4$ cm for $U_\infty = 10{\cdot}1$ m/s ($R_{ex} = 5{\cdot}96 \times 10^5$) of figure 9, one finds good agreement in the general shape of the two wall-pressure traces. However, while the magnitudes of C_p for the first positive and central negative peaks are nearly equal, the second positive peak of Savas ($\xi = 0{\cdot}65$) has a maximum value of $C_p \simeq 0{\cdot}018$ as compared to $C_p \simeq 0{\cdot}005$ for the present measurement. The location of the two positive peaks in Savas' data occur at $\xi = 0{\cdot}80$ and $\xi = 0{\cdot}65$, as compared to $\xi_p = 0{\cdot}83$ and $\xi_p = 0{\cdot}54$ in figure 9. When Savas' data is replotted in terms of the pressure-signature virtual origin (x_{0p}, t_{0p}), the two positive peaks shift to $\xi = 0{\cdot}81$ and $\xi = 0{\cdot}55$, and the resulting pressure signature corresponds more closely to the present measurements. Unfortunately it is not possible to obtain a pressure virtual origin from Savas' data as the above results indicate a sensitivity of the comparison to the choice of virtual origin.

Savas (1979), in his figure 28, presented the relationship between C_p and the ensemble velocity intermittency contours at the spot's half-height in terms of the spatial co-ordinate Ut. The comparison shows that the two pressure maxima occur after passage of the spot's velocity-disturbance leading and trailing interfaces, and that the pressure minimum is associated with the central region of the spot. These results are consistent with the location of the pressure maxima in ξ_p and lend validity to the use of a pressure virtual origin in transforming the pressure data into similarity co-ordinates.

Neither the present measurements nor that of Savas agree with the results of DeMetz & Casarella (1973), who measured the velocity and wall-pressure fluctuations occurring during natural transition on a flat plate. Their data was typically high-pass filtered, represented in terms of intermittency and based on measurements at unknown locations within spots occurring randomly during natural transition. No detailed studies of the wall-pressure signature characteristics were made, but DeMetz & Casarella concluded that the shapes of the velocity and pressure fields were similar (their figure 26) and that the pressure bursts have leading and trailing edge celerities of $0{\cdot}97\,U_\infty$ and $0{\cdot}31\,U_\infty$ respectively. The causes of these discrepancies with the present measurements is unclear.

The C_p data when compared to the ensemble-mean velocity data of Cantwell *et al.* and Wygnanski *et al.* produce several interesting relationships. The longitudinal velocity near the wall is increasingly positive throughout passage of the spot, showing a sharp increase at the leading edge and a maximum at the trailing interface. Because the increase in velocity near the wall implies a steep normal gradient $\partial u/\partial y$, the skin friction should increase accordingly and Wygnanski *et al.* report that the gradient of $\partial u/\partial y$ as $y \to 0$ increases toward the trailing edge. If the wall-pressure field were directly related to the shear stress τ_0 at the wall, then the leading- and trailing-edge pressure maxima would be related to the steep velocity changes near the wall.

It has been reported (e.g. Blake 1970) that in the fully turbulent boundary layer, the pressure fluctuations at a point are produced mainly by local velocity fluctuations

and that the dominant contribution to the mean-square pressure is produced by the interaction of the turbulence and the mean shear. In the absence of pressure gradients, the wall shear is the only external stress and, according to Blake (1970), this stress apparently determines the level of fluctuating pressure exerted at the wall by eddy motion in the boundary layer. Blake and others have concluded that the r.m.s. pressure is related to the shear stress by $\bar{C}_p = 2(\overline{P^2})^{\frac{1}{2}}/\rho U_\infty^2 \simeq 3{\cdot}4C_f$, which yields typical values of $\bar{C}_p \simeq 0{\cdot}0025$ and $\bar{C}_p \simeq 0{\cdot}013$ for laminar and turbulent boundary layers respectively, and $\bar{C}_p \simeq 0{\cdot}01$ for individual spot-pressure realizations. If the results of the fully turbulent boundary layer can be applied to the turbulent spot, one might conjecture that the two positive peaks along the centre line are due to shear stresses induced by two vortices within the spot whose location may coincide with the two stable particle-path foci calculated by Cantwell *et al.* The increasing negative region of the pressure field corresponds with the increase in spatial growth of the nearly constant shear region produced in the body of the spot by the velocity excess near the wall. Experimental data concerning the wall shear stress would be a useful contribution in the determination of the pressure–velocity interactions.

Contour plots were constructed for the ensemble C_p data in terms of the similarity co-ordinates ξ_p and ζ_p, where $\zeta_p = z/U_\infty(t-t_{0p})$. The contour plots for $U_\infty = 7{\cdot}8$ and $10{\cdot}1$ m/s are shown in figures 11 and 12 respectively. The C_p contours present the spot's ensemble pressure signatures as an arrowhead-shaped structure consisting of three distinct regions each bounded by a 10% deviation from ambient, where the central pressure-defect region is preceded and followed by regions of pressure excess. The C_p contours for $U_\infty = 7{\cdot}8$ and $10{\cdot}1$ m/s have the same degree of similarity as the individual C_p traces in figure 9. If a universally similar pressure signature were to exist then the C_p contours would be similar for all x and U_∞; however, the contours show that the geometry of the pressure field is evolving as it is convected downstream. The leading region of pressure excess is found to be larger for $U_\infty = 10{\cdot}1$ m/s, but it is reduced in size and more closely contained along the centre line for increasing x. The pressure-defect region becomes increasingly constant and less negative near the centre line, with the region of large pressure defect moving outward and becoming concentrated in the wing-tip region. The streamwise width of the spanwise coherent trailing-edge pressure-excess region narrows in ξ_p with increasing x, and has its pressure maxima concentrated around $\zeta_p = \pm 0{\cdot}06$ ($z/b \simeq 0{\cdot}6$). The effect of Reynolds number on streamwise spatial growth is shown by the larger size of both the leading pressure-excess and pressure-defect regions and by the earlier arrival of the leading excess contours and later passage of trailing excess contours for $U_\infty = 10{\cdot}1$ m/s. The maximum spanwise growth is approximately the same for both velocities.

From the spanwise distribution of the three velocity components and velocity correlations, Wygnanski *et al.* (1976) concluded that the turbulent spot contains a large arrowhead-shaped vortex tube that dominates flow within the spot, and that near the centre line the vorticity is concentrated near the leading and trailing edges. They further concluded that the vortex tube narrows with increasing z, causing the emergence of a well-defined spanwise vortex and the disappearance of the central 'calm' region. In their model, the concept of a narrowing vortex in the spanwise direction would explain the reduction and final disappearance of the first pressure maximum with increasing z while the trailing-edge pressure peak remains strong and coherent in z. For increasing z, the central pressure minimum sharpens and increases

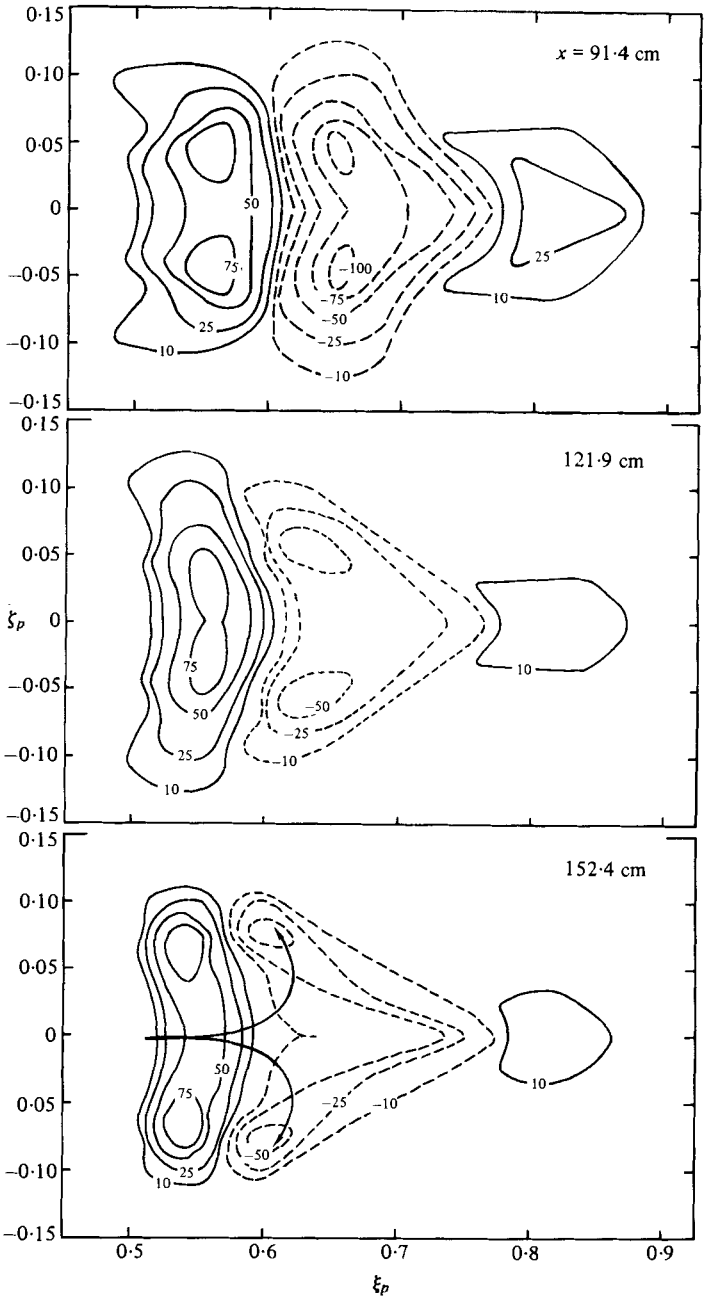

FIGURE 11. Contour map of the ensemble-mean $C_p \times 10^4$ in similarity co-ordinates (ξ_p, ζ_p) for $U_\infty = 7{\cdot}8$ m/s relative to ambient. Arrows represent conceptual view of fluid entrainment.

to a maximum negative peak at $z/b \simeq 0{\cdot}50$–$0{\cdot}75$ and may be attributed to the combination of the motion of the locus of minimum-U points moving toward the trailing edge at large z, the maximum spanwise W-velocity component at $z/b \simeq 0{\cdot}75$, and the concentration of the sharply negative (toward the wall) V-velocity at the leading edge with increasing z. The dynamics of the pressure field are consistent with the

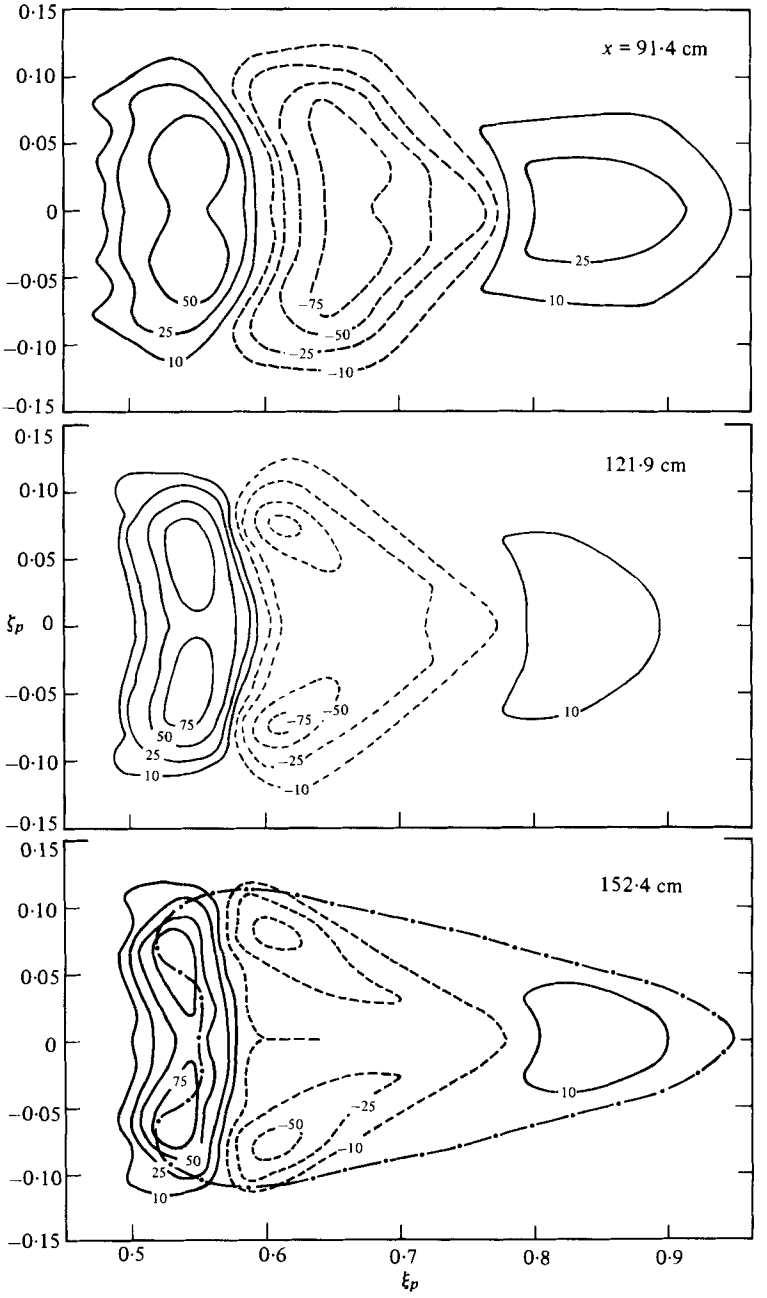

FIGURE 12. Contour map of the ensemble-mean $C_p \times 10^4$ in similarity co-ordinates (ξ_p, ζ_p) for U_∞ = 10·1 m/s relative to ambient. · — ·, zero r.m.s. contour.

swept-back vortex concept and, while the central negative region shows streamwise growth with increasing x, the general characteristics of the wall-pressure signature are stable with respect to position and velocity.

The C_p contours show that as the spot is convected downstream, the central pressure-defect region evolves into a region of low pressure along the centre line, with a concen-

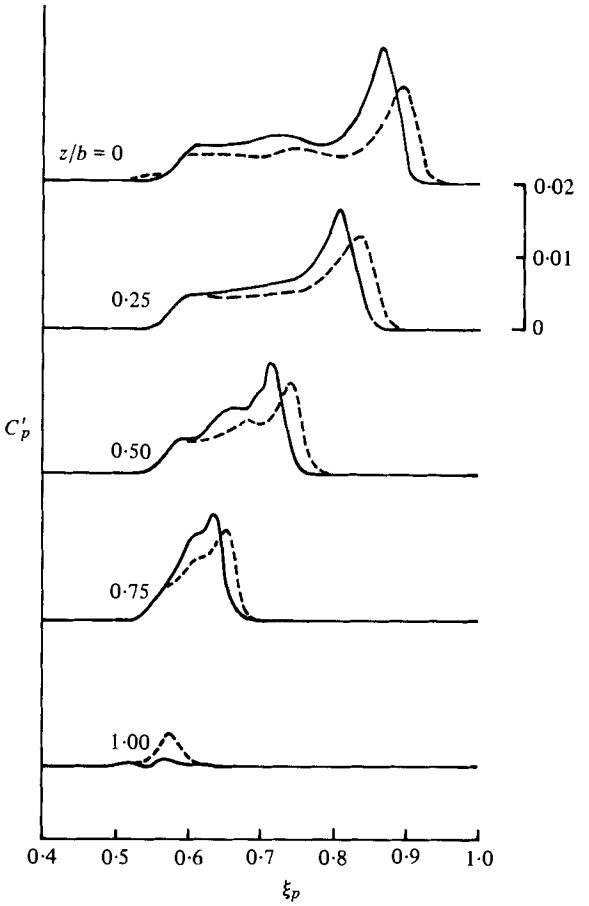

FIGURE 13. Ensemble-averaged wall-pressure fluctuations C'_p as functions of ξ_p for $x = 152{\cdot}4$ cm. ——, $U_\infty = 7{\cdot}8$ m/s; – – –, 10·1 m/s.

tration of maximum pressure defect at the wing tips, producing a favourable pressure gradient in the outward z-direction. At the same time, the trailing-edge pressure-excess region evolves into a region having a maximum pressure excess at the wing tips, producing an unfavourable pressure gradient in the z-direction. The type of vortical motion due to the entrainment of fluid postulated by Wygnanski *et al.* would produce this type of pressure distribution, resulting in fluid being drawn away from the centre line and accelerated in the z-direction. The arrows in figure 11 show, conceptually, the path of the entrained fluid as it enters the centre of the trailing edge and is accelerated outward toward the wing tips.

An interesting correspondence exists between the particle paths of Cantwell *et al.* (1978), the velocity-perturbation contours of Zilberman, Wygnanski & Kaplan (1977) and the C_p contours. The maxima and minima of the velocity-disturbance contours appear to be associated with both the stable foci or particle-path accumulation points 1 and 2 in figure 10 and the trailing edge of the initial pressure-excess and pressure-defect regions (i.e. the $C_p = \pm 0{\cdot}001$ contours). Along the centre line, the first pressure minimum occurs prior to the focus at $\xi = 0{\cdot}77$ and the second pressure maximum occurs after the focus at $\xi = 0{\cdot}64$, placing the central negative region

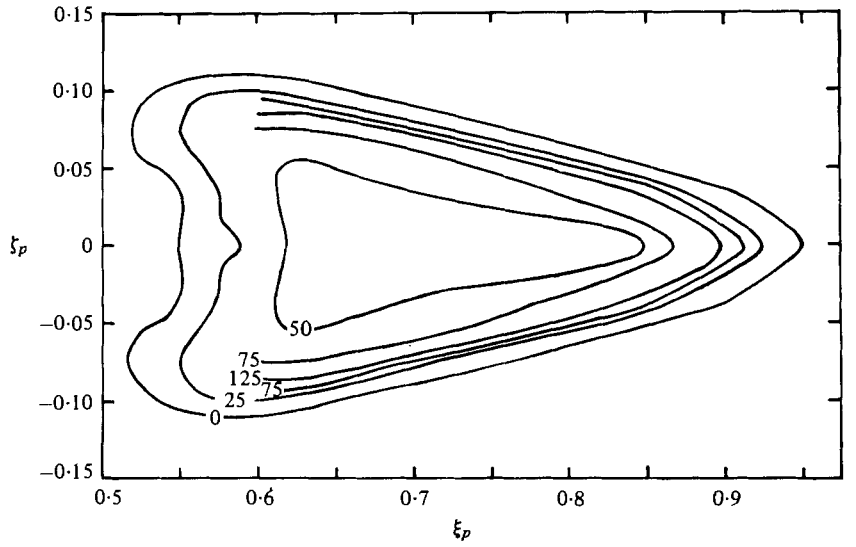

FIGURE 14. Contour map of the ensemble-averaged $C'_p \times 10^4$ in similarity co-ordinates (ξ_p, ζ_p) for $U_\infty = 10{\cdot}1$ m/s at $x = 152{\cdot}4$ cm relative to ambient ($C'_p = 0$).

between the two foci. The velocity-defect region outlined by the $-2\,\%\ U_\infty$ contours extends from $\xi = 0{\cdot}6$ to $0{\cdot}9$, which is the region occupied by the initial C_p, excess and central defect contours. The velocity-excess region, outlined by the $+2\,\%\ U_\infty$ contour, extends along the entire length of the spot's wall-pressure contours. As can be seen, there is no direct one-to-one correspondence between the velocity and pressure contours along the centre line.

The ensemble-mean C'_p signatures at $x = 152{\cdot}4$ cm are shown in figure 13 as functions of ξ_p for five values of z/b. Along the centre line, the C'_p traces show a sharp increase to a maximum just prior to the arrival to the first positive-pressure peak. The C'_p maximum is followed by a rapid decrease to a plateau value that persists through the central region of the wall-pressure signature and then sharply decreases before the arrival of the second positive-pressure perturbation. For increasing z/b, the central plateau is reduced in length and the C'_p signature becomes characterized by a single peak in the wing-tip region. It can also be seen from figure 13 that the similarity co-ordinate ξ_p does not completely collapse the C'_p traces for $U_\infty = 7{\cdot}8$ and $10{\cdot}1$ m/s. The Reynolds-number effect observed in the C_p signatures (figure 9) appears to be more pronounced in the C'_p data, and a reduction in magnitude of C'_p occurs for increasing Reynolds number.

A contour plot of the r.m.s. pressure fluctuations C'_p at $x = 152{\cdot}4$ cm and $U_\infty = 10{\cdot}1$ m/s is represented in figure 14 in terms of the similarity co-ordinates (ξ_p, ζ_p). The zero r.m.s. contour ($C'_p = 0$, laminar region) not only exhibits the characteristic turbulent-spot arrowhead shape but also encloses nearly all the C_p contours, as shown in figure 12. The largest fluctuation level coincides with the $C_p = 0{\cdot}001$ contour along the centre line and more closely coincides with the spot's leading edge for increasing z/b, finally terminating in the wing-tip region of maximum C_p defect. The central region of the spot is characterized by a fairly uniform fluctuation level that decreases rapidly and extends through the region coinciding with the coherent trailing-edge positive-pressure peak. Even though the region preceding the arrival of the wall-

pressure field's leading edge undergoes large fluctuations about the ensemble mean, the central plateau region of both C_p and C'_p act as if the conditions of a fully turbulent boundary layer were present within the spot followed by a rapid adjustment to the 'calm' region behind the spot.

5. Conclusions

The ensemble-mean C_p signatures show that the wall-pressure signature of a turbulent spot consists of two positive-pressure perturbation regions and a central negative-pressure region that becomes relatively flat for large x. For increasing z/b, the wall-pressure field becomes characterized by one negative- and one positive-pressure peak. Transformation of the pressure signatures C_p and C'_p into the similarity co-ordinates (ξ_p, ζ_p) shows a Reynolds-number dependence in the spatial growth and fluctuation levels. The C_p contours show that both the central pressure defect and trailing-edge pressure excess have their respective maxima in the wing-tip region.

The authors acknowledge the support of the Naval Ocean Systems Center's Independent Research Program. Additionally, C. W. Van Atta acknowledges the support of NSF Grant Eng 78-25088.

REFERENCES

BLAKE, W. 1970 Turbulent boundary-layer wall-pressure fluctuations on smooth and rough walls. *J. Fluid Mech.* **44**, 637–660.

BULL, M. 1967 Wall-pressure fluctuations associated with subsonic turbulent boundary layer flow. *J. Fluid Mech.* **28**, 719–754.

CANTWELL, B., COLES, D. & DIMOTAKIS, P. 1978 Structure and entrainment in the plane of symmetry of a turbulent spot. *J. Fluid Mech.* **87**, 641–672.

COLES, D. & SAVAS, O. 1980 Interactions for regular patterns of turbulent spots in a laminar boundary layer. In *Proc. IUTAM Symp. on Laminar-turbulent Transition, Stuttgart, September* 1979 (ed. R. Eppler & H. Fasel), pp. 277–287. Springer.

DEMETZ, F. & CASARELLA, M. 1973 An experimental study of the intermittent properties of a boundary layer pressure field during transition on a flat plate. *NSRDC Rep.* no. 4140.

GEDNEY, C. 1979 Wall pressure fluctuations during transition on a flat plate. *M.I.T. Acoustics and Vibration Lab. Rep.* no. 84618-1.

HUANG, T. & HANNAN, D. 1975 Pressure fluctuations in the region of flow transition. *DTNSRDC Rep.* no. 4723,

SAVAS, O. 1979 Some measurements in synthetic turbulent boundary layers. Ph.D. thesis, California Institute of Technology.

SCHUBAUER, G. & KLEBANOFF, P. 1956 Contributions on the mechanics of boundary layer transition. *N.A.C.A. Rep.* no. 1289.

WILLMARTH, W. 1975 Pressure fluctuations beneath turbulent boundary layers. *Ann. Rev. Fluid Mech.* **7**, 13–38.

WYGNANSKI, I., SOKOLOV, M. & FRIEDMAN, D. 1976 On a turbulent spot in a laminar boundary layer. *J. Fluid Mech.* **78**, 785–819.

ZILBERMAN, M., WYGNANSKI, I. & KAPLAN, R. 1977 Transitional boundary layer spot in a fully turbulent environment. *Phys. Fluids. Suppl.* **20**, 258–271.